Nondegenerate Parametric Resonance in Large Ensembles of Coupled Micromechanical Cantilevers with Varying Natural Frequencies

Christopher B. Wallin, Roberto De Alba, Daron Westly, Glenn Holland, Scott Grutzik, Richard H. Rand, Alan T. Zehnder, Vladimir A. Aksyuk, Slava Krylov, and B. Robert Ilic

Phys. Rev. Lett. **121**, 264301 — Published 28 December 2018

DOI: 10.1103/PhysRevLett.121.264301

Nondegenerate Parametric Resonance in Large Ensembles of Coupled MEMS Cantilevers with Varying Natural Frequencies

Christopher B. Wallin,[1,2] Roberto De Alba,[1,2] Daron Westly,[1] Glenn Holland,[1] Scott Grutzik,[3] Richard H. Rand,[4,5] Alan T. Zehnder,[4] Vladimir A. Aksyuk,[1] Slava Krylov,[6] and B. Robert Ilic[1,*]

[1]*Physical Measurement Laboratory, National Institute of Standards and Technology, Gaithersburg, MD 20899, USA*

[2]*Institute for Research in Electronics and Applied Physics, University of Maryland, College Park, MD 20742, USA*

[3]*Component Science and Mechanics, Sandia National Laboratories, Albuquerque, NM 87185, USA*

[4]*Sibley School of Mechanical and Aerospace Engineering, Cornell University, Ithaca, NY 14853, USA*

[5]*Department of Mathematics, Cornell University, Ithaca, NY 14853, USA*

[6]*School of Mechanical Engineering, Faculty of Engineering, Tel Aviv University, Ramat Aviv 69978 Tel Aviv Israel*

Abstract

We investigate the collective dynamics and nondegenerate parametric resonance (NPR) of coplanar, interdigitated arrays of microcantilevers distinguished by their cantilevers having linearly expanding lengths and thus varying natural frequencies. Within a certain excitation frequency range, the resonators begin oscillating via NPR across the entire array consisting of 200 single-crystal silicon cantilevers. Tunable coupling generated from fringing electrostatic fields provides a mechanism to vary the scope of the NPR. Our experimental results are supported by a reduced-order model that reproduces the leading features of our data including the NPR band. The potential for tailoring the coupled response of suspended mechanical structures using NPR presents new possibilities in mass, force, and energy sensing applications, energy harvesting devices, and optomechanical systems.

With the emergence of micro and nanoelectromechanical (M/NEMS) systems in recent decades, M/NEMS resonator arrays have been increasingly employed in the practical study of the complex, collective behavior of coupled oscillator systems. Large arrays of coupled MEMS resonators were first reported in the seminal work of Buks and Roukes [1], whereby 67 electrostatically coupled, doubly clamped beams produced rather unanticipated responses. Instead of featuring 67 collective vibrational modes, their nonlinear responses exhibited a small number of asymmetric resonance peaks, which were broad relative to the expected mode spacing, extended beyond their predicted band edges, and displayed abrupt pattern switching behavior. Subsequently, M/NEMS resonator arrays have been shown to exhibit a host of nontrivial dynamics due predominantly to their nonlinear nature including intrinsically localized modes [2–4], multistability and hysteresis [5], and synchronization [6–8]. The applicability of these M/NEMS resonator arrays also has been wide-ranging and includes signal processing applications such as radio frequency (RF) filtering [9] and frequency conversion [10], oscillator phase noise reduction through synchronization for enhanced clocking and frequency stability [11–14], and ultrasensitive mode-localized sensing [15–18]. Many of these effects and their derived applications fundamentally depend on the complicated interplay between various constituents of the array due to coupling mechanisms which are generally mediated elastically [19–21], optically [22–24], or electrostatically [1, 25–27]. While theoretical investigations into large degree of freedom resonator arrays commonly focus on the system's response to changes in coupling parameters and natural frequencies [6, 28–30], experimental implementation of such devices remains challenging because they usually require complicated coupling topologies and complex readout transduction schemes. Nonetheless, device realization of globally tunable coupled array systems is relatively straightforward, especially with electrostatic coupling which does not necessitate additional piezoelectric or optical device layers.

Customarily, the electrostatic coupling or drive configurations in M/NEMS systems naturally give rise to parametric excitation and resonance through time-dependent, nonlinear electrostatic forces which effectively create modulating spring constants. Utilizing electrostatic parametric resonance in M/NEMS structures has become ubiquitous principally due to its capability of producing resonant responses when excited at frequencies other than at the system's natural frequency, along with the ease of implementation. These systems are routinely described by a generalization of Mathieu's equation, namely the nonlinear Hill's

equation. It is well known that Mathieu's equation has parametric instability tongues that exist near frequencies $f = 2f_j^{NM}/k$ where f_j^{NM} is a j^{th} natural frequency of the system, $k = 1, 2, \ldots$, and the superscript NM denotes a normal mode [31]. These critical frequency values represent fundamental parametric resonance of order k and have been explored in M/NEMS systems for reasonably high values of k despite the fact that higher-order resonances progressively have exponential narrowing of their instability regions [32, 33].

Further possibilities of parametric resonance exist in multi-degree of freedom systems where the possibility of mutual interaction of eigenmodes exists. Nondegenerate parametric resonance (NPR), also known as combination parametric resonance [31], occurs in neighborhoods near frequency values $f \approx (f_j^{NM} \pm f_l^{NM})/k$ for $j, l = 1, 2, \ldots$ and $k = 1, 2, \ldots$ where f_j^{NM} and f_l^{NM} correspond to distinct normal modes of the system. In general, NPR emerges in systems with time-dependent mode couplings, which results in frequency mixing and parametric resonant responses at sums or differences of the system's natural frequencies. While NPR has been well studied theoretically [31, 35, 36], actual implementation of NPR in M/NEMS systems has been limited [37–42] and has not been observed in large M/NEMS arrays to the best of our knowledge.

In this Letter, we consider both theoretically and experimentally the complex behavior and NPR of coupled, parametrically driven, interdigitated arrays of microcantilevers with linearly changing cantilever lengths. More specifically, we describe herein the array-spanning, summed-type NPR that occurs over a wide frequency band due to the distinctive spatially confined mode structure and the associated natural frequency distribution resulting from the geometry of the device.

As shown in Fig. 1(a), the device is comprised of two opposing, partially interdigitated cantilever arrays with 100 cantilevers apiece. Each array has cantilever lengths expanding linearly across the device in opposite directions with a maximum length of $L_{max} \approx 500$ μm and a minimum length of $L_{min} \approx 350$ μm. The width and thickness of the cantilevers are $b \approx 20$ μm and $h \approx 5$ μm respectively. Additional device parameters include the gap length between neighboring counter-orientated cantilevers, the length of the compliant overhang, and the length of the overlap region. These parameters respectively correspond to $g \approx 5$ μm, $L_o \approx 100$ μm, and $L_e \approx 150$ μm. Fabrication process details can be found in [43].

In the overlap region, electrostatic coupling is generated through the asymmetries in the fringing fields between neighboring cantilevers and serves to produce an electrostatic

restoring force as illustrated in Fig. 1(b). The electrostatic force per unit length in the overlap region defined by $L_n - L_e \leq \hat{y} \leq L_n$, acting on the n^{th} cantilever, $F_n^e(\hat{y}, \hat{t})$, can be approximated by [43]

$$F_n^e = \alpha\sigma\hat{V}^2\left(\frac{\frac{\hat{w}_{n+1}-\hat{w}_n}{h}}{1+\sigma|\frac{\hat{w}_{n+1}-\hat{w}_n}{h}|^{2p}} - \frac{\frac{\hat{w}_n-\hat{w}_{n-1}}{h}}{1+\sigma|\frac{\hat{w}_n-\hat{w}_{n-1}}{h}|^{2p}}\right), \tag{1}$$

where $\hat{w}_n(\hat{y})$ is the out-of-plane defection of the n^{th} beam and $\hat{V}(\hat{t})$ is the time dependent voltage applied across the arrays. The remaining terms, α, σ, and p, are geometry-dependent fitting parameters which were found to be $\alpha = 2.45 \times 10^{-6}$ $\mathrm{N \cdot mV^{-2}}$, $\sigma = 0.133$, and $p = 1.191$. In order to motivate the possibility of NPR actuation within the device, further examination of Eq. (1) is necessary. Assuming $\hat{V}(\hat{t}) = \hat{V}_{ac}\cos(\omega_D\hat{t})$ where ω_D is the excitation angular frequency, we find after linearizing Eq. (1) that the electrostatic force per unit length can be approximated by

$$F_n^e \approx \frac{\alpha\sigma}{h}\frac{\hat{V}_{ac}^2}{2}\Big(1 + 2\cos(2\omega_D\hat{t})\Big)\Big(\hat{w}_{n+1} - 2\hat{w}_n + \hat{w}_{n-1}\Big). \tag{2}$$

Eq. (2) represents a coupled Mathieu-type term [31] which produces k^{th} order NPR excitation at critical NPR frequencies $f = 2f_D \approx (f_j^{NM} + f_l^{NM})/k$.

In order to experimentally investigate the dynamics of the arrays, the devices were fixed on a stage in a vacuum chamber (VC) at pressure of $\approx 10^{-3}$ Pa as depicted in Fig. 1(c). The out-of-plane motion of the cantilevers was observed using an optical setup consisting of a 1× long working distance objective (LWDO), a fiber-optic illuminator (FOI), a beam splitter (BS), a zoom lens (ZL), and a camera (CAM). Each measurement involved applying a time-varying voltage undergoing a linearly chirped frequency sweep given by $\hat{V}(\hat{t}) = \hat{V}_{ac}\cos[2\pi(f_0\hat{t} \pm k\hat{t}^2/2)]$ to one array while grounding the opposing array. This time-varying voltage was produced by a function generator (FG) and a high voltage amplifier (HVA). With f_0 being the starting chirp frequency, the drive signal was either up-chirped or down-chirped over a range of ≈ 26 kHz to ≈ 56 kHz at a rate of $k \approx 107$ Hz/s. Since the camera has a frame rate of ≈ 30 $\mathrm{s^{-1}}$, the captured data only gives a qualitative estimate to the magnitude of a beam's deflection time-averaged over many oscillation periods. As Fig. 1(d) highlights, large cantilever deflections scatter light more readily, leaving their image noticeably darker relative to non-oscillating cantilevers. The estimated vibrational amplitude of each cantilever was determined by the associated grayscale pixel values at the ends

of the beams. Pixel averaging was performed over 20 pixels to reduce the noise in the measurement and background subtraction was performed to reduce errors caused by nonuniform illumination of the sample. Modal pattern maps were generated by obtaining the grayscale pixel values from each video frame and concatenating them together across frequency space as Fig. 1(e) exemplifies. These experimental modal patterns shown in Fig. 1(e) primarily resemble the normal mode shapes predicted by FE analysis as presented in Fig. 1(f).

While the measurement technique described above is straightforward and provides qualitative estimates for the normal mode shapes and relative vibrational amplitudes, a consequential drawback of its simplicity is that it only gives the system's response at a specified drive frequency and provides no direct measurement of the oscillation frequency of the individual cantilevers. Experimental verification of first-order NPR actuation in the arrays requires that the first-order NPR frequency condition, $f_D \approx (f_j^{NM} + f_l^{NM})/2$, be satisfied and appropriately measured, which is a challenging proposition considering our limited frequency measurement capabilities. In order to circumvent this difficulty, the measured NPR mode shapes were cross-correlated with the measured normal mode shapes. Assuming that the normal modes oscillate at the drive frequency, this procedure gives an estimate of the frequency response of the NPR modes. As shown in Fig. 2(a) and 2(b), the down-chirped response at $\hat{V}_{ac} \approx 40$ V produced 15 distinct NPR modes, which are highlighted in the insets. The normal modes responsible for these excited NPR modes were determined by finding the region within the modal pattern map which gave the maximum 2-dimensional cross-correlation with a given NPR mode in a specified array. The analysis was performed across the entire frequency space outside of the NPR band and was subject to the constraint that the cantilevers remain aligned to themselves. As an example of the results obtained from the described procedure, Figs. 2(c)–2(h) show the strong similarity between NPR mode 8 and the matching normal modes.

With the NPR-generating normal modes identified, cantilever-averaged resonance curves were used to find the peak resonant frequencies of the j^{th} normal mode in Array 1, $f_j^{NM,1}$, and the l^{th} normal mode in Array 2, $f_l^{NM,2}$. Additionally, the peak resonant frequencies of the m^{th} NPR mode for Array 1 , $f_m^{NPR,1}$, and Array 2, $f_m^{NPR,2}$, were found for their respective cantilever-averaged resonance curves. These frequencies, $f_m^{NPR,1}$ and $f_m^{NPR,2}$, are not the oscillation frequency of the NPR modes, but the drive frequency at which the NPR modes have peak resonance. All peak locations were determined by fitting a localized quadratic

polynomial using the method of least squares. As shown in Fig. 2(i), the frequency deviation from the NPR frequency condition was calculated by $\Delta f = f_j^{NM,1} + f_l^{NM,2} - 2f_D$, where we have taken $f_D = (f_m^{NPR,1} + f_m^{NPR,2})/2$ to be the drive frequency averaged about the NPR peak resonances in both of the arrays. The maximum observed frequency deviation from ideal NPR frequency condition for all the modes was less than 15 Hz, which conclusively demonstrates that the modes were excited via the NPR mechanism.

Additional experiments were performed at higher voltages to explore the effects of the nonlinearities and the expanded parametric instability regions produced from the stronger coupling constant. Figure 3 shows the frequency response at $\hat{V}_{ac} \approx 56$ V and $\hat{V}_{ac} \approx 81$ V using a down-chirped drive. At $\hat{V}_{ac} \approx 56$ V, many NPR modes were actuated, especially along the periphery of the device, as the critical coupling strength was achieved for parametric instability. As the drive voltage was increased to ≈ 81 V, a well-defined NPR band from ≈ 34 kHz to ≈ 42 kHz formed and nearly all the cantilevers were oscillating to some degree. The extent of the NPR actuation directly depended on the applied voltage, which is consistent with Eqs. (1) and (2).

To explain the dynamics more rigorously, a reduced-order (RO) model was developed using the Galerkin decomposition under the direction of Euler-Bernoulli beam theory [26, 34]. Full details of the RO model are described in the Supplemental Material. Numerical solutions were generated by solving the RO model's system of equations describing the dynamics of each individual beam using Runge-Kutta methods. As shown in Fig. 4(a), the simulated modal patterns qualitatively display many of the observed experimental features. Additional analysis on the spatial and temporal dynamics of the arrays using the RO model and spectral analysis further confirmed NPR actuation within our system. Power spectral densities using Welch's method were calculated for each frequency step in the numerical solution and concatenated together to form spectrograms. Whereas cantilevers near the center of the arrays were principally driven by fundamental parametric resonance within the NPR band, cantilevers near the periphery of the arrays were excited strictly by NPR within the NPR band and followed the relation $f_D \approx (f_j^{NM} + f_l^{NM})/2$ for the j^{th} and l^{th} modes as indicated by the responses of beams 10 and 11 in Figs. 4(b)–4(d). A similar analysis was performed on other adjacent beams within the array, and this provided further confirmation that the excitation of the beams outside of the spatially confined normal modes in the NPR band was principally due to the NPR mechanism.

In this Letter, we have demonstrated NPR excitation in large arrays of coupled, interdigitated MEMS cantilevers. The distinctive device topology produced spatially confined mode structures with mode-to-mode coupling between opposing arrays, which permitted efficient NPR actuation within the NPR frequency band. Exploiting NPR in future engineered M/NEMS systems could facilitate device operation at a multitude of frequencies, possibly enabling bandwidth expansion through frequency conversion and greater tunability of M/NEMS devices for applications such as resonance based sensing. Furthermore, these arrays could potentially be utilized as a nondegenerate parametric amplifier by applying a small-signal at f_j^{NM} to one array while pumping at $f_D \approx (f_j^{NM} + f_l^{NM})/2$ on the opposing array leading to signal amplification and phase noise reduction [44]. The high sensitivity of these coupled arrays to environmental perturbations will likely open new and interesting sensing scenarios based on NPR-actuated collective pattern recognition rather than on the frequency monitoring of individual elements.

This work was performed in part at the Physical Measurement Laboratory (PML) and the Center for Nanoscale Science and Technology (CNST) at the National Institute of Standards and Technology (NIST) and the Cornell NanoScale Facility, a member of the National Nanotechnology Coordinated Infrastructure (NNCI), which is supported by the National Science Foundation (Grant ECCS-1542081). This work was partially supported by the National Science Foundation (Grant CMMI 1634664). Sandia National Laboratories is a multimission laboratory managed and operated by National Technology & Engineering Solutions of Sandia, LLC, a wholly owned subsidiary of Honeywell International Inc., for the U.S. Department of Energy's National Nuclear Security Administration under contract DE-NA0003525. S. Krylov acknowledges support from the Henry and Dinah Krongold Chair of Microelectronics. Christopher B. Wallin and Roberto De Alba acknowledge support under the Cooperative Research Agreement between the University of Maryland and the National Institute of Standards and Technology Center for Nanoscale Science and Technology, Award 70NANB14H209, through the University of Maryland. This paper describes objective technical results and analysis. Any subjective views or opinions that might be expressed in the paper do not necessarily represent the views of the U.S. Department of Energy or the United States Government.

* robert.ilic@nist.gov

[1] E. Buks and M. L. Roukes, Journal of Microelectromechanical Systems **11**, 802 (2002).

[2] M. Sato, B. E. Hubbard, A. J. Sievers, B. Ilic, D. A. Czaplewski, and H. G. Craighead, Physical Review Letters **90**, 044102 (2003).

[3] M. Sato, B. E. Hubbard, and A. J. Sievers, Reviews of Modern Physics **78**, 137 (2006).

[4] E. Kenig, B. A. Malomed, M. C. Cross, and R. Lifshitz, Physical Review E **80**, 046202 (2009).

[5] R. Lifshitz and M. C. Cross, Physical Review B **67**, 134302 (2003).

[6] M. C. Cross, J. L. Rogers, R. Lifshitz, and A. Zumdieck, Physical Review E **73**, 036205 (2006).

[7] S.-B. Shim, M. Imboden, and P. Mohanty, Science **316**, 95 (2007).

[8] D. K. Agrawal, J. Woodhouse, and A. A. Seshia, Journal of Applied Physics **115**, 164904 (2014).

[9] C. T. C. Nguyen, IEEE Transactions on Ultrasonics, Ferroelectrics, and Frequency Control **54**, 251 (2007).

[10] K. R. Qalandar, B. S. Strachan, B. Gibson, M. Sharma, A. Ma, S. W. Shaw, and K. L. Turner, Applied Physics Letters **105**, 244103 (2014).

[11] C. Heng-Chia, C. Xudong, U. K. Mishra, and R. A. York, IEEE Transactions on Microwave Theory and Techniques **45**, 604 (1997).

[12] M. H. Matheny, M. Grau, L. G. Villanueva, R. B. Karabalin, M. C. Cross, and M. L. Roukes, Physical Review Letters **112**, 014101 (2014).

[13] M. Zhang, S. Shah, J. Cardenas, and M. Lipson, Physical Review Letters **115**, 163902 (2015).

[14] F. Torres, A. Uranga, M. Riverola, G. Sobreviela, and N. Barniol, Sensors **16**, 1690 (2016).

[15] M. Spletzer, A. Raman, A. Q. Wu, X. Xu, and R. Reifenberger, Applied Physics Letters **88**, 254102 (2006).

[16] M. Spletzer, A. Raman, H. Sumali, and J. P. Sullivan, Applied Physics Letters **92**, 114102 (2008).

[17] P. Thiruvenkatanathan, J. Yan, J. Woodhouse, A. Aziz, and A. A. Seshia, Applied Physics Letters **96**, 081913 (2010).

[18] C. Zhao, M. H. Montaseri, G. S. Wood, S. H. Pu, A. A. Seshia, and M. Kraft, Sensors and

Actuators A: Physical **249**, 93 (2016).

[19] M. Sato, B. E. Hubbard, L. Q. English, A. J. Sievers, B. Ilic, D. A. Czaplewski, and H. G. Craighead, Chaos: An Interdisciplinary Journal of Nonlinear Science **13**, 702 (2003).

[20] M. Sato and A. J. Sievers, Physical Review Letters **98**, 214101 (2007).

[21] O. Takahito, T. Keitaro, and K. Yusuke, Journal of Micromechanics and Microengineering **24**, 025012 (2014).

[22] M. Zhang, G. S. Wiederhecker, S. Manipatruni, A. Barnard, P. McEuen, and M. Lipson, Physical Review Letters **109**, 233906 (2012).

[23] M. Bagheri, M. Poot, L. Fan, F. Marquardt, and H. X. Tang, Physical Review Letters **111**, 213902 (2013).

[24] E. Gil-Santos, M. Labousse, C. Baker, A. Goetschy, W. Hease, C. Gomez, A. Lemaitre, G. Leo, C. Ciuti, and I. Favero, Physical Review Letters **118**, 063605 (2017).

[25] P. Thiruvenkatanathan, J. Yan, J. Woodhouse, and A. A. Seshia, Journal of Microelectromechanical Systems **18**, 1077 (2009).

[26] S. Krylov, S. Lulinsky, B. R. Ilic, and I. Schneider, Applied Physics Letters **105**, 071909 (2014).

[27] P. N. Kambali, G. Swain, A. K. Pandey, E. Buks, and O. Gottlieb, Applied Physics Letters **107**, 063104 (2015).

[28] M. C. Cross, A. Zumdieck, R. Lifshitz, and J. L. Rogers, Physical Review Letters **93**, 224101 (2004).

[29] J. F. Rhoads, S. W. Shaw, and K. L. Turner, Journal of Dynamic Systems, Measurement, and Control **132**, 034001 (2010).

[30] P. Cudmore and C. A. Holmes, Chaos: An Interdisciplinary Journal of Nonlinear Science **25**, 023110 (2015).

[31] A. H. Nayfeh and D. T. Mook, *Nonlinear oscillations* (Wiley, New York, 2008).

[32] K. L. Turner, S. A. Miller, P. G. Hartwell, N. C. MacDonald, S. H. Strogatz, and S. G. Adams, Nature **396**, 149 (1998).

[33] Y. Jia, S. Du, and A. A. Seshia, Scientific Reports **6**, 30167 (2016).

[34] N. Dick, S. Grutzik, C. B. Wallin, B. R. Ilic, S. Krylov, and A. T. Zehnder, Journal of Vibration and Acoustics **140**, 051013 (2018).

[35] A. H. Nayfeh and D. T. Mook, The Journal of the Acoustical Society of America **62**, 375

(1977).

[36] A. A. Mailybayev and A. P. Seyranian, Journal of Applied Mathematics and Mechanics **65**, 755 (2001).

[37] B. Rajashree and K. L. Turner, Journal of Micromechanics and Microengineering **13**, 701 (2003).

[38] M. Napoli, Z. Wenhua, K. Turner, and B. Bamieh, Journal of Microelectromechanical Systems **14**, 295 (2005).

[39] H. Okamoto, A. Gourgout, C.-Y. Chang, K. Onomitsu, I. Mahboob, E. Y. Chang, and H. Yamaguchi, Nature Physics **9**, 480 (2013).

[40] I. Mahboob, H. Okamoto, K. Onomitsu, and H. Yamaguchi, Physical Review Letters **113**, 167203 (2014).

[41] Y. S. Patil, S. Chakram, L. Chang, and M. Vengalattore, Physical Review Letters **115**, 017202 (2015).

[42] S. Cho, S. U. Cho, M. Jo, J. Suh, H. C. Park, S. G. Kim, S.-B. Shim, and Y. D. Park, Physical Review Applied **9**, 064023 (2018).

[43] Y. Linzon, B. Ilic, S. Lulinsky, and S. Krylov, Journal of Applied Physics **113**, 163508 (2013).

[44] A. Olkhovets, D. W. Carr, J. M. Parpia, and H. G. Craighead, in *Technical Digest. MEMS 2001. 14th IEEE International Conference on Micro Electro Mechanical Systems*, pp. 298–300.

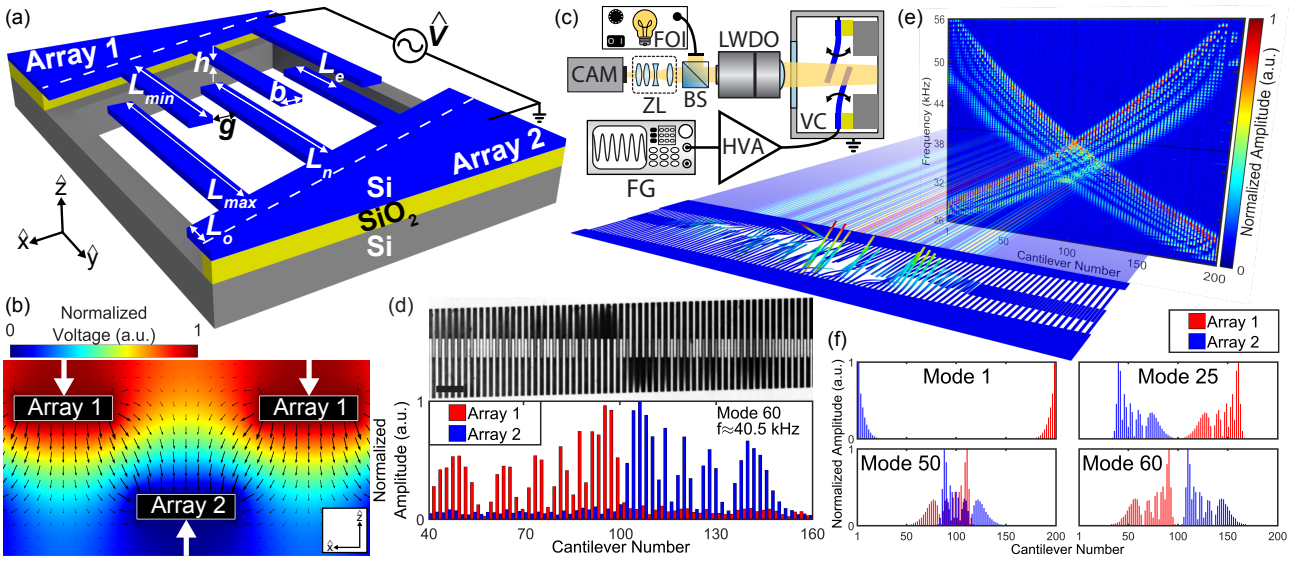

FIG. 1. (a) Schematic of the interdigitated, variable length microcantilever arrays. The actual device has 200 cantilevers. Electrostatic coupling between oppositely-oriented, nearest-neighbor cantilevers is generated via fringing electrostatic fields in the overlap region designated by L_e. Long-range mechanical coupling is produced in each array's overhang, which is defined by L_o and delineated by the dotted lines on Array 1 and Array 2. (b) Results from finite element (FE) analysis illustrating the fringing electrostatic field between adjacent cantilevers in the overlap region. This field provides a restoring force between neighboring beams as indicated by the white arrows. The lengths of the black arrows are proportional to the electric field strength at the given locations. (c) Schematic of the experimental setup. (d) An optical micrograph (top) of the center of the device being actuated at a drive frequency of $f_D \approx 40.5$ kHz. The scale bar is 100 μm. The spatially averaged grayscale pixel values (bottom) are obtained from the end of each cantilever providing a qualitative estimate of the out-of-plane vibrational amplitude for every cantilever on the device. (e) Modal patterns are developed by concatenating together the response at each frequency step [26]. The rendered image of a device consisting of 200 oscillating cantilevers shows explicitly the mapping of the device dynamics at $f_D \approx 40.5$ kHz to an experimentally obtained modal pattern. For the sake of clarity of the mapping, the experimental modal pattern was specifically chosen to consist only of the normal modes of the system and to exhibit no NPR. (f) Normalized amplitudes of various spatially localized modes generated from a full-scale FE modal analysis [34]. Spatial overlap of the opposing arrays' modes is a necessary condition for NPR excitation in the system.

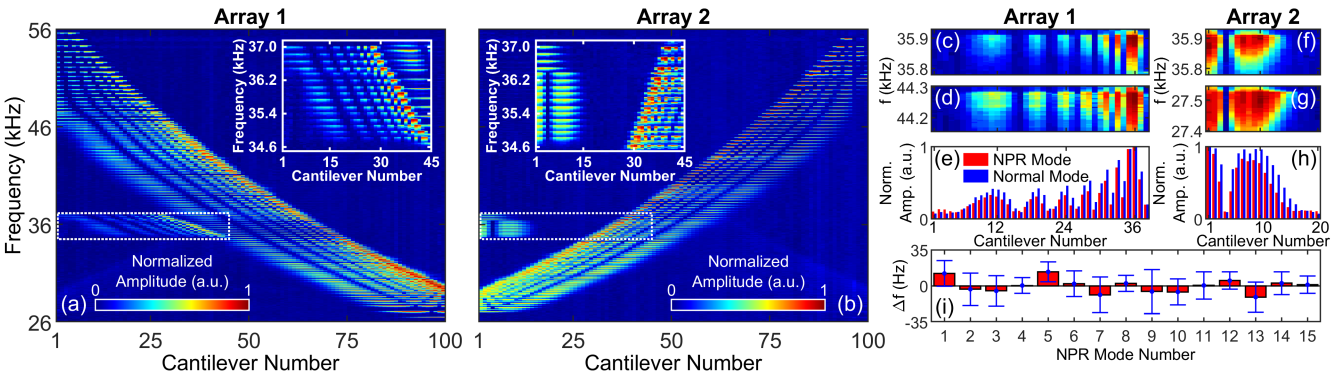

FIG. 2. The frequency response and NPR excitation of (a) Array 1 and (b) Array 2 driven at $\hat{V}_{ac} \approx 40$ V, which is marginally above the NPR threshold voltage. 15 NPR modes are featured within the dotted rectangles and are replotted in their respective insets. As an example of the results obtained from the normal mode matching algorithm, we have (c) NPR mode 8 and (d) the maximally correlated normal mode, both from Array 1, showing almost indistinguishable mode structures. (e) Modal shapes produced by summing over frequency space using Array 1's NPR mode 8 and its maximally correlated normal mode, further indicating nearly identical features. (f) NPR mode 8, (g) the maximally correlated normal mode, and (h) the modal shapes, all from Array 2, illustrating strong similarity between the two modes. (i) The frequency deviation, Δf, from the NPR frequency condition conclusively demonstrates that the 15 modes outlined above are excited via the NPR mechanism. The error bars correspond to 95% confidence intervals. All plots involving normalized amplitudes (Norm. Amp.) are normalized independently.

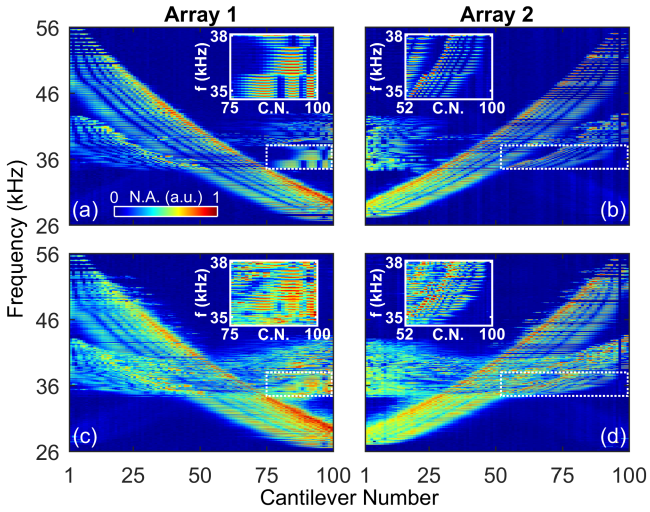

FIG. 3. The down-chirped frequency response at $\hat{V}_{ac} \approx 56$ V for (a) Array 1 and (b) Array 2 showing the emergence of a NPR band spanning across all cantilever numbers (C.N.). The insets highlight 22 NPR modes. Nonlinearities start to influence the dynamics significantly at $\hat{V}_{ac} \approx 81$ V as presented in (c) and (d) for Array 1 and Array 2, respectively. All plots are normalized independently and use the same normalized amplitude (N.A.) colormap.

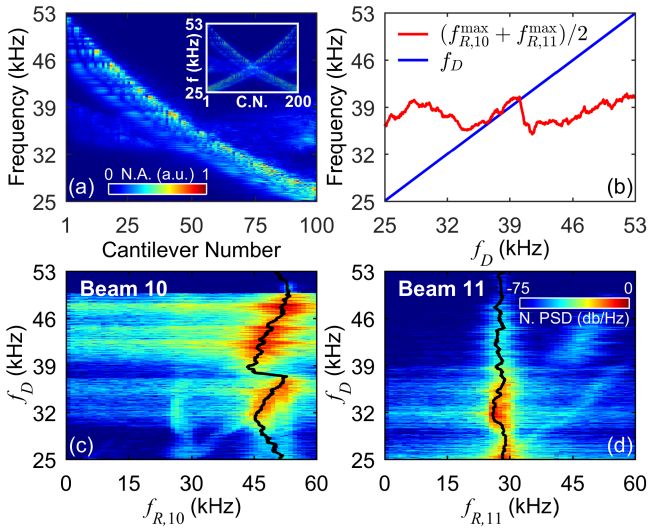

FIG. 4. (a) The calculated down-chirped frequency response with $\hat{V}_{ac} = 100$ V showing a NPR band from ≈ 33 kHz to ≈ 40 kHz. The inset depicts the response of both arrays. (b) Summation of the numerically calculated peak frequency response for beams 10 and 11. Within the NPR region, the summed peak frequency response of beam 10, $f^{\max}_{R,10}$, and beam 11, $f^{\max}_{R,11}$, follow the relation $f_D \approx (f^{\max}_{R,10} + f^{\max}_{R,11})/2$. The spectrograms of (c) beam 10 and (d) beam 11 computed using Welch's power spectral density (PSD) method along with the associated 9 point moving-average filtered peak frequency response shown as black lines. Both plots use the same normalized PSD colormap.